ACS APPLIED MATERIALS & INTERFACES

Research Article

www.acsami.org

Controllable Synthesis of Hierarchical Porous Fe_3O_4 Particles Mediated by Poly(diallyldimethylammonium chloride) and Their Application in Arsenic Removal

Ting Wang,[†] Liyuan Zhang,[†] Haiying Wang,[†,‡] Weichun Yang,[†,‡] Yingchun Fu,[§] Wenli Zhou,[§] Wanting Yu,[†] Kaisong Xiang,[†] Zhen Su,[†] Shuo Dai,[†] and Liyuan Chai*[,†,‡]

[†]Department of Environmental Engineering, School of Metallurgy and Environment, Central South University, Changsha 410017, P. R. China

[‡]Chinese National Engineering Research Center for Control & Treatment of Heavy Metal Pollution, Changsha 410017, P. R. China

[§]Key Laboratory of Chemical Biology and Traditional Chinese Medicine Research (Ministry of Education), College of Chemistry and Chemical Engineering, Hunan Normal University, Changsha 410081, P. R. China

Supporting Information

ABSTRACT: Hierarchical porous Fe_3O_4 particles with tunable grain size were synthesized based on a facile poly (diallyldimethylammonium chloride) (PDDA)-modulated solvothermal method. The products were characterized with scanning electron microscopy (SEM) and transmission electron microscopy (TEM), X-ray photoelectron spectroscopy (XPS), Fourier transform infrared spectroscopy (FT-IR), X-ray diffraction (XRD), N_2 adsorption−desorption technique, vibrating sample magnetometer (VSM), and dynamic light scattering (DLS). The results show that increasing the PDDA dosage decrease the grain size and particle size, which increased the particle porosity and enhanced the surface area from 7.05 to 32.75 $m^2\ g^{-1}$. Possible mechanism can be ascribed to the PDDA function on capping the crystal surface and promoting the viscosity of reaction medium to mediate the growth and assembly of grain. Furthermore, the arsenic adsorption application of the as-obtained Fe_3O_4 samples was investigated and the adsorption mechanism was proposed. High magnetic Fe_3O_4 particles with increased surface area display improved arsenic adsorption performance, superior efficiency in low-level arsenic removal, high desorption efficiency, and satisfactory magnetic recyclability, which are very promising compared with commercial Fe_3O_4 particles.

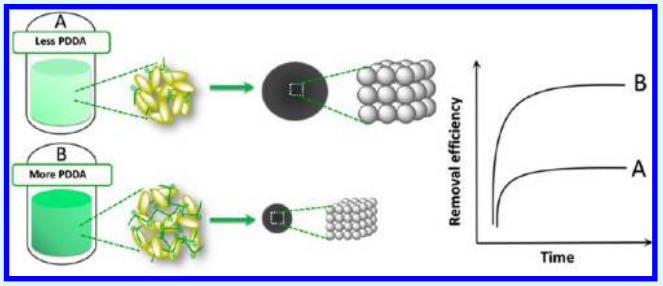

KEYWORDS: *Fe_3O_4, poly (diallyldimethylammonium chloride), solvothermal, adsorption*

1. INTRODUCTION

Arsenic, one of the top 20 hazardous substances, greatly threatens the health of human body, ecological balance, and industrial development.[1] Thus, the remediation of arsenic pollution has attracted worldwide attention.[2−4] So far, technologies involving oxidation,[5] coagulation,[6] adsorption,[7−9] ion-exchange,[10] and reverse osmosis[11] have been developed to detoxicate arsenic pollution. Among them, adsorption is one of the most promising technologies for arsenic removal, because of its easy operation and low-cost production.[4,12,13] However, the separation of traditional adsorbent (e.g., filtration, centrifugation or gravitational sedimentation) is time-consuming and cost-ineffective and therefore limits the practical application.[14] Hence, magnetic adsorbents such as Fe_3O_4 exhibit unique advantages due to their quick and effective magnetic separation.[15−17]

In parallel, the rapid growth of nanotechnology has attracted a great deal of interest in environmental application.[18−25] In terms of the application of Fe_3O_4 as an adsorbent, decreasing the Fe_3O_4 particle size from micrometers to nanometers would increase the available adsorptive areas by 100 to 1000 times.[26−28] However, as the Fe_3O_4 particle size decreases to nanometers, its response to an external magnetic field undesirably decreases, which will not be large enough to overcome Brownian motion and no efficient magnetic separation will occur.[26,29,30] To tackle this problem, one practical strategy is to prepare magnetic hierarchical structures, which are constructed with building blocks of nanounits. The hierarchical nanostructures not only exhibit high specific surface area because of the abundant interparticle spaces or intraparticle pores, but also possess satisfactory magnetic response because of their larger size and weaker Brownian motion, which therefore show great superiority to individual nanometer- and micrometer-sized materials.[31−36] To date, two conventional

Received: August 22, 2013
Accepted: November 19, 2013

   dx.doi.org/10.1021/am403533v | ACS Appl. Mater. Interfaces XXXX, XXX, XXX−XXX

template methods were reported to synthesize hierarchical nanoarchitectures, including hard templates such as silica,[37] polymer spheres,[38] and metal oxides,[39] as well as soft templates such as emulsion droplets/micelles[40,41] and even gas bubbles.[42] These synthetic routes seem to be inconvenient because complicated template presynthesis or time-consuming precursor calcination at elevated temperature is needed.[37,43−46] Moreover, the removal of templates by erosion or calcination brings adverse effect on the product morphology.[47,48] Consequently, it is preferable to develop one-step template-free methods for the preparation of hierarchical particles with well-defined morphology.

It is generally believed that the grain acts as the building block and its oriental assembly constitutes hierarchical particles. Consequently, it is predictable that the grain property and its assembly behavior synchronously influence product morphology.[49−51] To date, the reported advanced template-free methods have mainly focused on the modulation of grain assembly by Kirkendall effect,[52,53] Ostwald ripening effect[45,54−57] or self-attachment effect.[46,58,59] For instance, Yong et al. reported that the assembly of grain evolved into porous Fe_3O_4 hollow submicrospheres based on Ostwald ripening process through one-pot solvothermal method.[60] Though the pattern and mechanism of grain assembly were comprehensively investigated, rare researches were devoted to studying the effect of grain property on the performance of yielded Fe_3O_4 hierarchical particles.

Herein, our research aimed to controllably prepare Fe_3O_4 hierarchical particles via modulating the grain property though one-pot solvothermal method. To the best of our knowledge, reports have seldom demonstrated the availability of this strategy on controlling the morphology and application performance of hierarchical particles. Poly(diallyldimethylammonium chloride) (PDDA), as an environmentally friendly and low cost polyelectrolyte, has been widely used in the preparation of composites via electrostatic or $\pi-\pi$ stack interaction for biosensor and catalysis.[61−65] Although the potential modulation usage for the synthesis of magnetic particles has not been investigated. In this research, a facile PDDA-mediated solvothermal method was proposed to controllably synthesize Fe_3O_4 hierarchical particles. Increasing the PDDA dosage declines the grain and particle size, which leads to the increment of specific area and porosity, eventually enhancing the adsorption performance. The mechanism for PDDA-induced grain size tunable strategy was also discussed. The prepared Fe_3O_4 particles show higher adsorption capacity than commercial Fe_3O_4 particles and pose great potential in the low-level arsenic removal, such as the remediation of groundwater (with arsenic concentration of hundreds of micrograms per liter[66−68]).

2. EXPERIMENTAL SECTION

2.1. Materials. Ferric chloride hexahydrate ($FeCl_3·6H_2O$), anhydrous sodium acetate (CH_3COONa, NaAc), and ethylene glycol (EG) were obtained from the Sinopharm Group Chemical Reagent Co., Ltd.. A 35.0 wt % aqueous solution of high molar mass (M_w 100 000−200 000) PDDA was obtained from Sigma-Aldrich. $Na_3AsO_4·12H_2O$ and $NaAsO_2$ were used as the sources of As(V) and As(III), respectively. Commercial Fe_3O_4 with the diameter of 200 nm was purchased from Beijing Dk Nano technology Co., Ltd.. All reagents were used without further treatment. Ultrapure water with a resistivity of 18.2 MΩ cm^{-1}, produced with a Milli-Q apparatus (Millipore), was used throughout all of the experiments.

2.2. Preparation of Porous Fe_3O_4. Porous Fe_3O_4 particles were synthesized exploiting a facile solvothermal method via morphology-mediated by PDDA solution. In a typical procedure, 1.35 g of $FeCl_3·6H_2O$ was dissolved in a mixture containing 36 mL of EG and an appropriate amount of PDDA solution, then 3.6 g of NaAc was added. After vigorous stirring for 30 min, a transparent solution was obtained and transferred to a 50 mL Teflon-lined autoclave, which was then placed in an oven at 200 °C for 6 h, followed by naturally cooling to room temperature. The black precipitate was collected and ultrasonic washed by water and ethanol for three times, respectively, through magnetic separation. The yielded product was vacuum-dried at 60 °C for 12 h. By modulating the dosage of PDDA solution as 1, 2, 3, 4, 5, and 6 g, the resultant series products were separately named as Fe_3O_4-i (i = 1−6). To understand the formation mechanism of Fe_3O_4, Fe_3O_4-2 and Fe_3O_4-4 samples were collected at various reaction time (1.5, 2.5, 4, 5, 6, and 8 h), followed by washing and drying procedures. The obtained series products were denoted as Fe_3O_4-2-xh or Fe_3O_4-4-xh (x refers to the reaction time).

2.3. Characterization. Scanning electron microscopy (SEM, JSM-6360) and transmission electron microscopy (TEM, TECNAI G2) were used to characterize the morphology of the nanoparticles. The X-ray diffraction (XRD) patterns of the Fe_3O_4 were obtained using Rigaku D/Max-RB diffractometer with Cu−Kα radiation (λ = 0.15406 nm, 35 kV, 40 mA). X-ray photoelectron spectroscopy (XPS) measurements were carried out on a Thermo Fisher Scientific K-Alpha 1063 using Al Kα X-ray as the excitation source. Fourier 40 transformed infrared spectroscopy (FT-IR, Nicolet IS10) was employed to analyze the molecular structure of the yielded product at a resolution of 4 cm^{-1}. The size of the pinhole and the integration time were set as 100 μm and 30 s, respectively. Magnetic properties of the product were investigated using a vibrating sample magnetometer (VSM, EV7, ADE) with an applied field between −7000 and 7000 Oe at room temperature. Specific surface areas of the yielded products were measured by adsorption−desorption of ultrapure N_2 on a Quantachrome Instruments system via Brunauer−Emmett−Teller (BET) method. Pore size distribution was determined by N_2 desorption isotherm using Barret−Joymer−Halender (BJH) method. The size of the Fe_3O_4 particles was determined by dynamic light scattering (DLS) on a Malvern zetasizer instrument (type Nano-ZS, Malvern Instruments Ltd., Britain) using Fe_3O_4 suspension with the concentration of 0.01 g L^{-1}.

2.4. Batch Adsorption Experiment. Solutions containing different concentrations of As(V) or As(III) were prepared and adjusted to pH 5 ± 0.2 using HCl. Then, 5 mg of the adsorbent sample was added to 10 mL arsenic aqueous solution under stirring. After a specified time, the solid and liquid were magnetic separated and the initial and residual concentrations of arsenic were measured by inductively coupled plasma-optical emission spectroscopy (ICP-OES) (Optima 5300DV). The adsorption isotherm was obtained by varying the initial arsenic concentrations and stirring for 4 h at 25 °C (concentration range: 0.1−17 mg L^{-1} for As(III) and 0.1−7.5 mg L^{-1} for As(V), respectively). For comparison, commercial Fe_3O_4 with the diameter of 200 nm synthesized by coprecipitation was also exploited. The equilibrium adsorption capacity (q_e) (mg g^{-1}) for arsenic was calculated according to the following equation

$$q_e = \frac{(c_0 - c_e)V}{m} \quad (1)$$

where c_0 and c_e (mg L^{-1}) are the initial and equilibrium arsenic aqueous concentrations, respectively; V is the volume (mL) of arsenic aqueous solution; m is the mass (mg) of adsorbents used in the experiment.

To test the low-level arsenic removal feasibility of adsorbents, initial arsenic solution with As(V) concentration in the range of 50−1400 μg L^{-1} and As(III) in the range of 50−600 μg L^{-1} were prepared. Other adsorption experiment procedures were the same as above.

The adsorption kinetics was investigated with the initial As(V) concentration of 3.5 mg L^{-1} and As(III) concentration of 3 mg L^{-1} at pH = 5.0 ± 0.2 and adsorbents dose = 0.5 g L^{-1}. The solution was

allowed to react with the adsorbent for a fixed period (between 10 and 240 min).

The regeneration of the absorbent was conducted by using 0.1 M NaOH solution as eluent with adsorbents dose = 1 g L^{-1} at 25 °C. Briefly, the absorbent was first ultrasonificated in NaOH solution for 30 min and then shaken for 2 h, followed by magnetic separation and washing by water three times. Then the adsorbent was applied into recycle adsorption study. The recycle adsorption experimental procedure and detection method are in accordance with the first adsorption experiment, including the mixing of the adsorbent with arsenic solution under stirring for 4 h, the solid and liquid separation by external magnetism, and the determination of the residual arsenic solution by ICP-OES (Optima 5300DV).

All the experimental data were the average of triplicate determinations with relative errors under 5%.

3. RESULTS AND DISCUSSION

3.1. Morphology, Structure, and Property of Fe_3O_4. The SEM images and size distribution of the Fe_3O_4-*i* (*i* = 1−6) particles are presented in Figure 1. As seen, Figure 1A−F shows

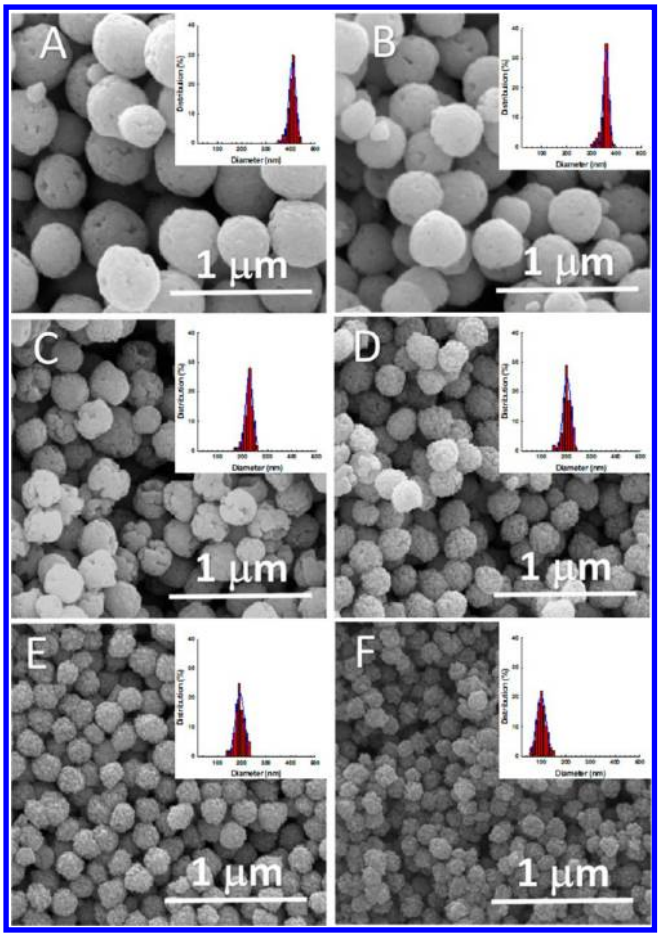

Figure 1. SEM images and the corresponding hierarchical particle size distribution of (A) Fe_3O_4-1, (B) Fe_3O_4-2, (C) Fe_3O_4-3, (D) Fe_3O_4-4, (E) Fe_3O_4-5, and (F) Fe_3O_4-6 at initial PDDA dosage varying from 1 to 6 g.

that the size of monodispersed hierarchical particles monotonously decreases from (A) 420 nm to (F) 100 nm, as increasing the PDDA dosage from 1 to 6 g. Correspondingly, the morphology of hierarchical particles gradually becomes coarse and porous, with the increase of PDDA dosage. As can be confirmed by TEM images in Figure S1 in the Supporting Information, increasing the PDDA dosage concurrently decreases hierarchical particle size and increases porosity. HRTEM images were also conducted to give further insight into the grain assembly, as shown in Figure 2. Taking Fe_3O_4-4 as an example, the particle shows pineal-like morphology with fringe spacing of 0.48 nm, corresponding to the (111) lattice planes of Fe_3O_4. The result indicates the possible oriented assembly of grain along (111) plane, which is the crystallographic plane with the highest energy and preferential for oriented attachment.[51] The structures and grain size of Fe_3O_4 were further measured by XRD, as shown in Figure 3. All the diffraction peaks at 18.32 ± 0.03, 30.10 ± 0.05, 35.48 ± 0.03, 43.10 ± 0.02, 53.40 ± 0.04, 57.02 ± 0.05, and 62.58 ± 0.08° can be indexed to the indices (111), (220), (311), (400), (422), (511), and (440) of Fe_3O_4. According to the Scherrer formula, the grain size gradually decreased from 34.4 nm (Fe_3O_4-2) to 13.4 nm (Fe_3O_4-6) with the increase of PDDA dosage (as listed in Table 1), which indicates the feasibility of the PDDA-induced grain size tunable strategy. Briefly speaking, the SEM, TEM, and XRD results show that PDDA modulated solvothermal method successfully modulate products morphology, particle size, grain size, and facilitate the oriented grain assembly.

On the other hand, the surface area and pore size distribution of as-synthesized Fe_3O_4-*i* (*i* = 2, 4, 5, 6) were determined by nitrogen adsorption−desorption measurements, as shown in Figure 4. Fe_3O_4-6 (Figure 4D) synthesized with the highest PDDA dosage possesses surface area and pore volume of 32.75 m^2 g^{-1} and 0.12 cm^3 g^{-1}, respectively, both of which are higher than that of the Fe_3O_4-5 (31.16 cm^2 g^{-1} and 0.117 cm^3 g^{-1}, Figure 4C), Fe_3O_4-4 (19.13 m^2 g^{-1} and 0.07 cm^3 g^{-1}, Figure 4B) and Fe_3O_4-2 (7.05 m^2 g^{-1} and 0.015 cm^3 g^{-1}, Figure 4A). All the samples pose pore size in the range of 7−12 nm. The results above can be ascribed to the fact that smaller grain assembly possesses more channels, leading to the increased surface area and pore amount. Hence, increasing the PDDA dosage yields Fe_3O_4 hierarchical particles composing of smaller grain, which exhibit higher surface area and porosity.

The magnetic property of Fe_3O_4 hierarchical particles was evaluated by examining the magnetic hysteresis loops at room temperature, as shown in Figure S2 in the Supporting Information. The M_s for the Fe_3O_4-*i* (*i* = 2−6) is in the range of 50−80 emu g^{-1}, which is comparable with many reported high magnetic particles.[31]

Briefly speaking, hierarchical porous Fe_3O_4 particles with high magnetism were synthesized by facile PDDA-modulated solvothermal method, which is achieved in one-pot solution reaction and avoids the time/energy consuming precursor calcination process. Furthermore, PDDA-induced grain size tunable strategy has been proved to be an efficient way to enhance the surface area and porosity of particles.

3.2. Mechanism for the Formation of Fe_3O_4 Hierarchical Particles Mediated by PDDA. The morphology and structure of the products with initial PDDA dosage of 4 g at various reaction time were examined by TEM, FT-IR and XRD to preliminarily understand the morphology and structure evolution of Fe_3O_4 hierarchical particles, as shown in Figure 5.

TEM results give insight into the morphology evolution of mesoporous Fe_3O_4. As shown in Figure 5A−F), three typical stages were observed for the formation of Fe_3O_4, namely, the formation of spindle precursor with length of 5−10 nm (0−1.5 h), the formation and assembly of grain to sphere particles (1.5−4 h), and the oriented assembly/Ostwald ripening

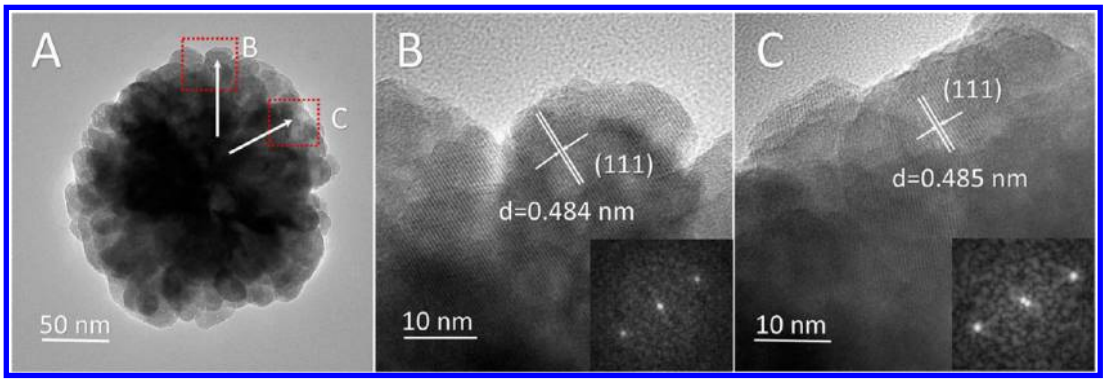

Figure 2. HRTEM images (A–C) of Fe_3O_4-4; B and C represent the magnification of the red area in A.

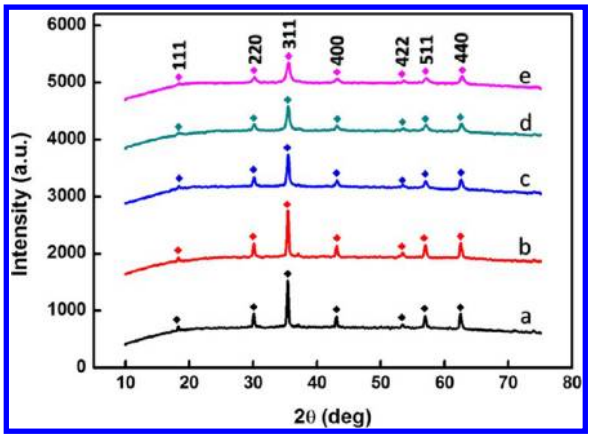

Figure 3. XRD patterns of Fe_3O_4 particles obtained at different PDDA dosage: (a) 2 g, (b) 3 g, (c) 4 g, (d) 5 g, (e) 6 g, with other experimental parameters keeping constant.

process of preformed sphere into porous particles (4–8 h). The XRD patterns (Figure 5G) of Fe_3O_4-4 at 1.5h depict a strong peak at 7.55° along with a broad weak one at 25° probably originated from (001) and (013) planes of an iron oxide acetate hydroxide hydrate with a formula of $Fe_2O(CH_3COO)(OH)_3 \cdot H_2O$ according to JCPDS.[69] Then XRD patterns of the samples obtained at the time from 2.5 to 4 h show gradually enhanced peaks at 30.00, 35.48, 43.14, 53.44, 57.04, and 62.58°, marked by the indices (220), (311), (400), (422), (511), and (440) of Fe_3O_4 phases. When the reaction time was 6–8 h, the produced aggregates were pure Fe_3O_4. The FT-IR spectra (Figure 5H) of Fe_3O_4-1.5h and Fe_3O_4-2.5h show reduced absorption peaks at 1578 and 1445 cm^{-1} due to the asymmetric and symmetric stretching of COO^- group, band at 1090 cm^{-1} owing to C–O stretching of the COO^- group, band at 887 cm^{-1} due to the OH bending.[69] The spectra of the samples within 4–8 h show broad strong band at 591 cm^{-1} due to the Fe–O lattice mode of Fe_3O_4.[34] Except for the anticipated typical peak for iron composite ($Fe_2O(CH_3COO)(OH)_3 \cdot H_2O$ or Fe_3O_4), the peak at 1125 cm^{-1} was ascribed to the C–N symmetric stretching vibration of PDDA. The PDDA also exhibits weak CH_2 bending vibrations (around 1474, 1326, and 960 cm^{-1}), C–H asymmetric, and C–H symmetric stretching frequencies (2918 and 2867 cm^{-1}).[70,71] Thus, both the XRD and FT-IR indicate the gradual formation of Fe_3O_4 phase at the expense of preformed $Fe_2O(CH_3COO)(OH)_3 \cdot H_2O$ phase.

Briefly speaking, typical three stages were observed for the formation of Fe_3O_4, namely, the formation of spindle precursor with length of 5–10 nm (mainly composed of $Fe_2O(CH_3COO)(OH)_3 \cdot H_2O$ at 0–1.5 h), the formation and assembly of grain to sphere Fe_3O_4 particles (1.5–4 h), and the oriented assembly/Ostwald ripening process of preformed sphere into porous Fe_3O_4 particles (4–8 h), which are in agreement with the reported literatures.[48,51,58,69,72] FT-IR analysis indicates that the hierarchical particles exhibit the vibration of PDDA which suggests the existence of PDDA on the particle surface and therefore the potential capping function of PDDA.

Furthermore, to reveal the effect of PDDA dosage on the morphology evolution, the amount was decreased from 4 to 2 g with otherwise the same conditions above, as shown in Figure S3 in the Supporting Information. The grains collected at 2.5, 4, 5, 6, and 8 h for the synthesis adopting 4 g of PDDA increase from 20.1 to 23.6 nm, indicating grain size increase by 3.5 nm; while the increment of grain size for the synthesis with 2 g of PDDA is 9.3 nm (increase from 21.5 to 30.8 nm). The results reflect that the increase in grain size was depressed as increasing the PDDA dosage, which might be partially ascribed to the capping effect of PDDA. On the other hand, it is discovered that the viscosity of the reaction medium was enhanced with the increase in PDDA dosage, as shown in Table 1. It is well-accepted that the increment of viscosity results in the promoted mass transfer resistance, which is not conductive to crystal growth, thus leading to the decreased grain size.[54,73]

Table 1. Viscosity of Reaction Medium, Particle Size, Grain Size, Magnetic Properties, And Absorption Performance of Fe_3O_4-*i* (*i* = 2–6) with different initial PDDA dosage

samples	PDDA dosage (g)	viscosity of reaction medium (Pa S)	particle size (nm)	grain size (nm)	magnetic property (emu g^{-1})	q_m (As(V)) (mg g^{-1})	q_e (As(III)) (mg g^{-1})
Fe_3O_4-2	2	0.062 ± 0.002	350 ± 15	34.4 ± 0.8	74.42 ± 1.93	1.93	1.57
Fe_3O_4-3	3	0.082 ± 0.004	215 ± 12	28.1 ± 0.6	72.11 ± 4.15	2.31	1.99
Fe_3O_4-4	4	0.106 ± 0.005	195 ± 10	20.2 ± 0.5	57.96 ± 3.47	4.07	3.29
Fe_3O_4-5	5	0.127 ± 0.004	185 ± 10	14.4 ± 0.3	53.96 ± 2.86	6.35	6.06
Fe_3O_4-6	6	0.145 ± 0.006	95 ± 10	13.3 ± 0.5	49.21 ± 3.13	7.23	6.77

dx.doi.org/10.1021/am403533v | ACS Appl. Mater. Interfaces XXXX, XXX, XXX–XXX

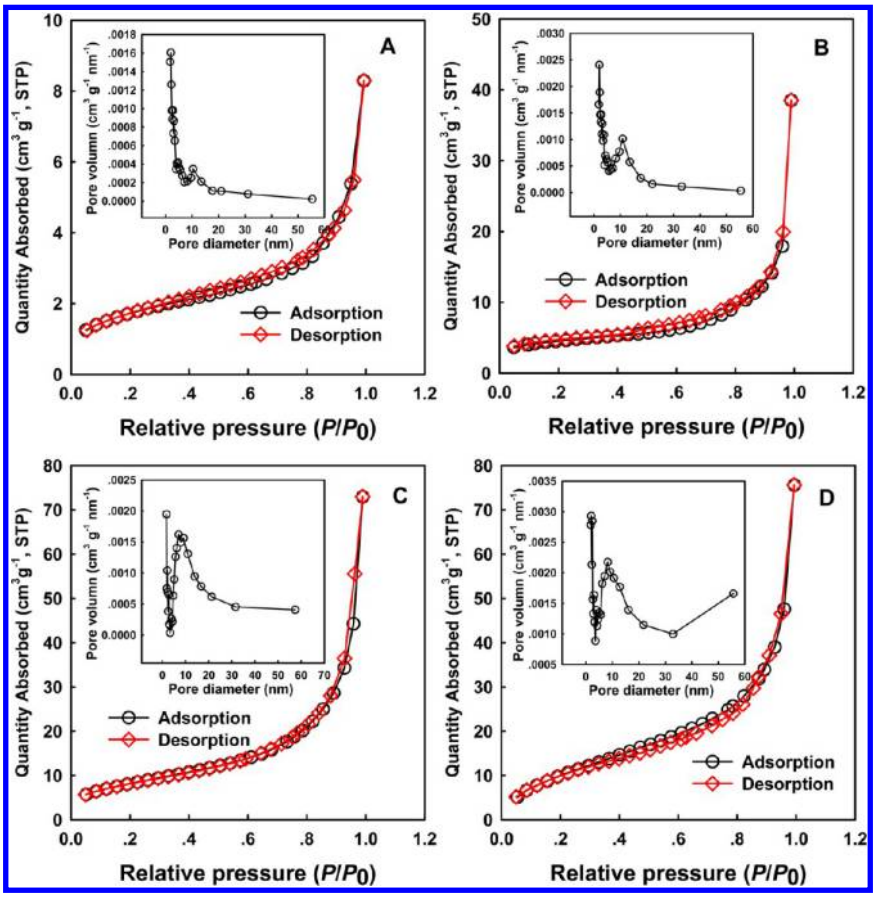

Figure 4. Nitrogen adsorption−desorption isotherms and pore-size distribution curves (the corresponding insert) of (A) as-obtained Fe_3O_4-2, (B) Fe_3O_4-4, (C) Fe_3O_4-5, and (D) Fe_3O_4-6, respectively.

Thus, based on the discussion above, a possible mechanism was proposed to elucidate the PDDA-induced grain size tunable strategy for the controllable synthesis of porous Fe_3O_4 hierarchical particles. As shown in Scheme 1, a mixture composed of $FeCl_3$, EG, NaAc, and PDDA was first obtained and the viscosity of mixture was greatly enhanced by PDDA. Spindle particles were then obtained with PDDA as capping agents, which improved the particle dispersibility. As time goes on, hierarchical Fe_3O_4 particles were eventually produced, and meanwhile PDDA function on capping effect and increasing viscosity declines particle and grain size, facilitates oriented assembly, thus synchronously enhancing surface area and porosity. Briefly speaking, a PDDA-modulated solvothermal method can controllably prepare porous Fe_3O_4 hierarchical particles.

3.3. Arsenic Adsorption Performance of Fe_3O_4. As discussed above, as-obtained Fe_3O_4 samples exhibit high specific area, high porosity, and excellent magnetic property, all of which are generally regarded as desirable properties of adsorbent for the pollutants removal. Before arsenic adsorption, the dispersibility of aqueous Fe_3O_4 samples was evaluated by determining the particle size via DLS. As shown in Figure S4 in the Supporting Information, the size of Fe_3O_4 shows a monotonous decrease from 520 nm (A) to 180 nm (F) with PDDA dosage from 1 to 6 g. Considering the possible plus bias for DLS compared with TEM/SEM,[74,75] the results indicate good dispersibility for Fe_3O_4 suspension. Then, the adsorption capacity of Fe_3O_4-i (i = 2−6) for As(V) and As(III) was evaluated using the equilibrium adsorption isotherm by varying the initial As(V) and As(III) concentrations. As shown in Figure 6A and C, the adsorption capacity of As(V) and As(III) monotonously increased from 1.93 and 1.57 mg g^{-1} for Fe_3O_4-2 to 7.23 and 6.77 mg g^{-1} for Fe_3O_4-6, indicating that the morphology mediated by PDDA greatly facilitates the absorption performance of particles. Fe_3O_4-5 and Fe_3O_4-6 in our research exhibit higher adsorption capacity than commercial Fe_3O_4 particles (1.35 mg g^{-1} for As(V) and 0.76 mg g^{-1} for As(III)) and some other reported metal oxide spheres, as listed in Table 2.[28,31,76] Moreover, in terms of the low contaminated drinking water (with hundreds of microgram per liter),[66] the prepared Fe_3O_4 exhibits excellent removal efficiency. Exploiting Fe_3O_4-5 as adsorbent, arsenic solution with initial As(V) concentration ≤800 μg L^{-1} or initial As(III) concentration ≤300 μg L^{-1} can be detoxicated to drinking water standard of USA (with arsenic concentration less than 10 μg L^{-1}) (see Figure S5 in the Supporting Information), indicating the potential application in the low-level arsenic removal.

Two equations, Langmuir and Freundlich isotherms models, were used to analyze the experimental data and the mathematical expressions are depicted in eq 2 and 3, respectively

$$\frac{C_e}{q_e} = \frac{1}{q_m K_L} + \frac{C_e}{q_m} \quad (2)$$

$$\log q_e = \frac{1}{n}\log c_e + \log K_F \quad (3)$$

dx.doi.org/10.1021/am403533v | ACS Appl. Mater. Interfaces XXXX, XXX, XXX−XXX

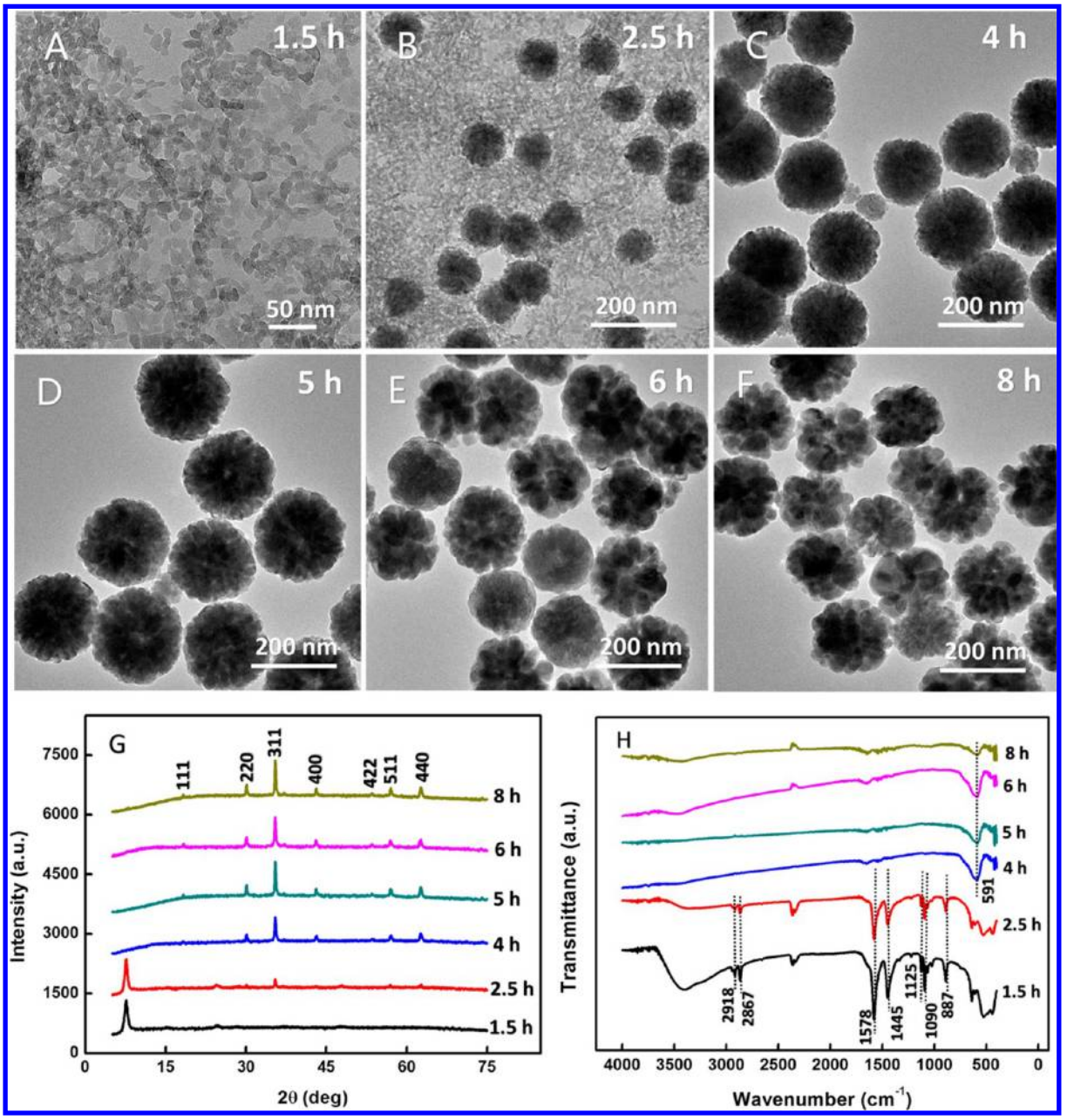

Figure 5. (A–F) TEM, (G) XRD, and (H) FT-IR spectra of Fe_3O_4-4-*x*h samples (*x* = 1.5, 2.5, 4, 5, 6, 8).

where q_m and K_L are Langmuir constants and represent the maximum adsorption capacity of adsorbents (mg g^{-1}) and the energy of adsorption, respectively. K_F and n are Freundlich constants related to adsorption capacity and adsorption intensity, respectively.

For the Langmuir isotherm model, the values of q_m and K_L can be calculated from the slope and intercept of plots of c_e/q_e versus c_e. For the Freundlich isotherm model, the values of n and K_F can be obtained by a plot of log q_e against log c_e. The adsorption of As(V) onto Fe_3O_4 fits the Langmuir isotherm model (Figure 6B), which interprets the adsorption process as a monolayer adsorption on a homogeneous surface. In contrast, the adsorption of As(III) onto Fe_3O_4 fits well with the Freundlich isotherm model (Figure 6D), indicating that the adsorption process is a multilayer adsorption on a homogeneous surface. The parameters of the Langmuir and Freundlich models were calculated and listed in Table S1 in the Supporting Information. The two different adsorption isotherm models may be attributed to the different surface charge effects of As(V) and As(III) species under the environment of pH 5.[77] For As(V), there exists an electrostatic attraction between positively charged Fe_3O_4 samples and negatively charged As(V) species and the adsorbed As(V) species have a repulsive effect on As(V) species in the solution. However, As(III) exists predominantly as noncharged H_3AsO_3.[7] The interaction between Fe_3O_4 samples and noncharged As(III) species is little so that the adsorption of As(III) should continue to increase with the increase of As(III) concentration.[77] Moreover, smaller $1/n$ implies stronger adsorption intensity.[31] Thus, the decrease of $1/n$ from Fe_3O_4-2 to Fe_3O_4-6 indicate that the adsorption process gradually becomes easier.

The kinetics of adsorption is one of the most important characteristics that define the adsorption efficiency, as shown in Figure 7. The adsorption of As(V) or As(III) is rapid at first

dx.doi.org/10.1021/am403533v | ACS Appl. Mater. Interfaces XXXX, XXX, XXX–XXX

Scheme 1. Scheme of the Formation of Hierarchical Fe_3O_4 Particles Mediated by PDDA

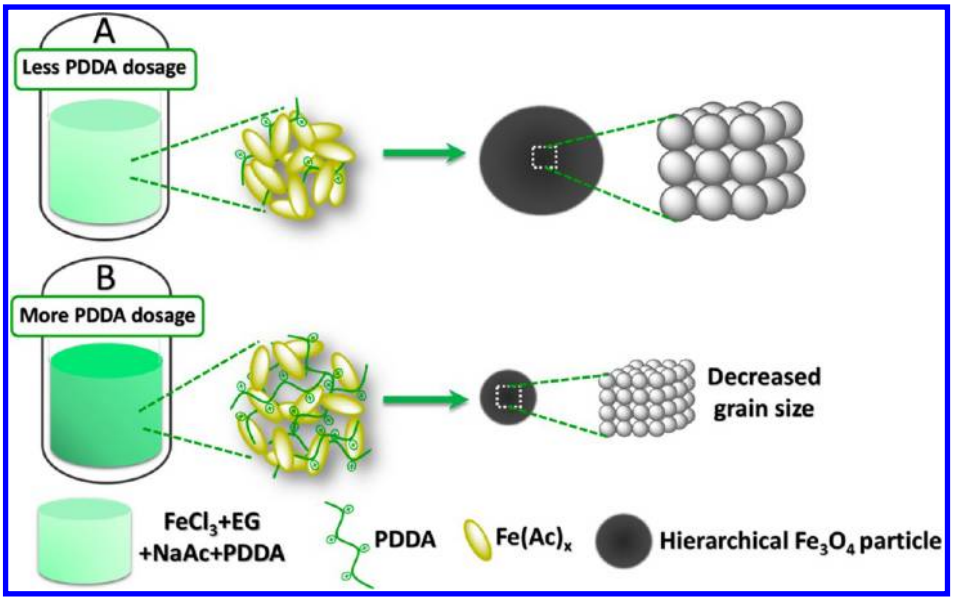

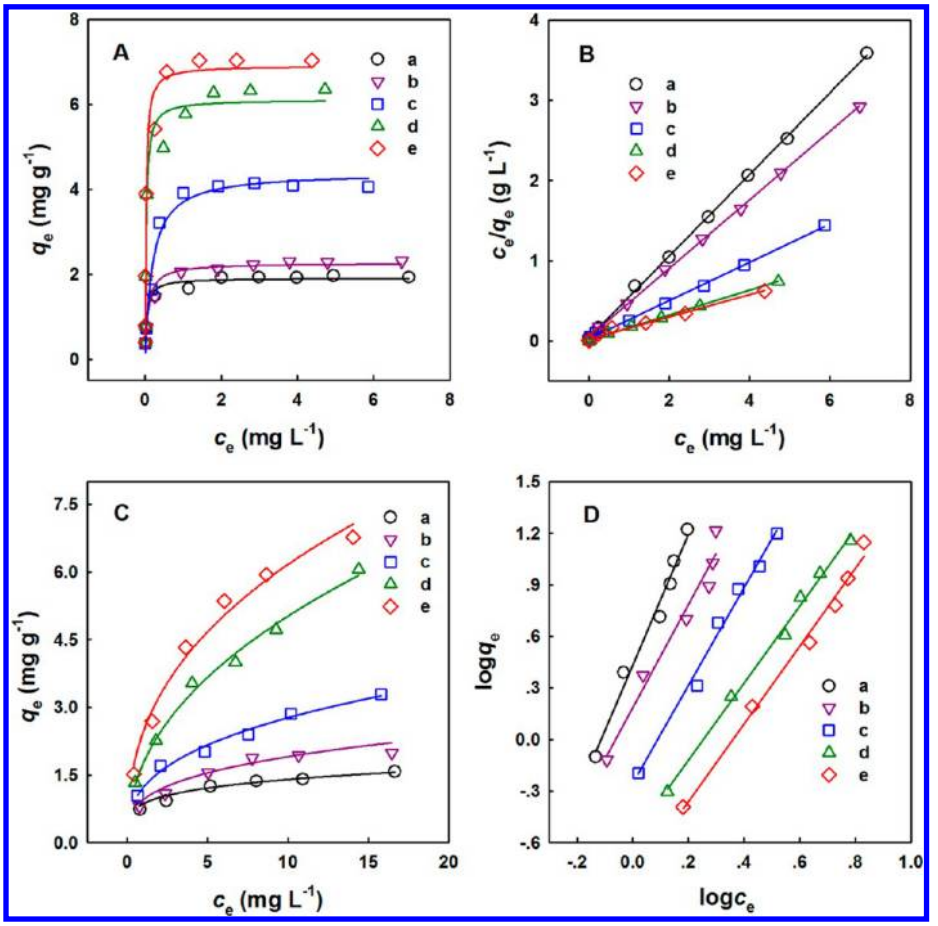

Figure 6. Adsorption isotherms of (A) As(V) and (C) As(III) onto (a) Fe_3O_4-2, (b) Fe_3O_4-3, (c) Fe_3O_4-4, (d) Fe_3O_4-5, and (e) Fe_3O_4-6 samples with the initial PDDA dosage of 2 g, 3 g, 4 g, 5 g, and 6 g, respectively. (B) Linearized Langmuir isotherm for As(V) adsorption and (D) linearized Freundlich isotherm for As(III) adsorption by (a) Fe_3O_4-2, (b) Fe_3O_4-3, (c) Fe_3O_4-4, (d) Fe_3O_4-5, and (e) Fe_3O_4-6 samples (T = 25 °C; adsorbent doses = 0.5 g L^{-1}; pH = 5 ± 0.2).

and then slows considerably. The rapid adsorption at first is ascribed to the process of arsenic adsorption on the exterior surface of the Fe_3O_4 particles. The slower adsorption rate followed might be partially due to the higher diffusion resistance as the arsenic begins to enter and move into the interior of the Fe_3O_4 particles via the nanopores.[77] Moreover, Fe_3O_4-5 exhibits the highest removal efficiency of 90.7% As(V) and 88.3% As(III), which are higher than Fe_3O_4-4 (57.3%

dx.doi.org/10.1021/am403533v | ACS Appl. Mater. Interfaces XXXX, XXX, XXX–XXX

Table 2. Comparison of the Adsorption Capacity of Arsenic on Fe_3O_4 with Reported Inorganic Oxide

adsorbent sample	pH	removal capacity for As(V) (mg g^{-1})	removal capacity for As(III) (mg g^{-1})	ref
Fe_3O_4-5	5	6.35	6.06	this work
Fe_3O_4-6	5	7.23	6.77	this work
Commercial Fe_3O_4	5	1.35	0.76	this work
porous α-Fe_2O_3	4	5.31		47
porous γ- Fe_2O_3	4	4.75		47
follow-like porous Fe_3O_4	4	4.65		47
chestnutlike Fe_3O_4 hierarchical nanstructure	4	6.07		31
cubic nickel frames		7.15		85
doughnut-like CuO	4		4.7	76
multilayer spherical CuO	4		0.5	76
Commercial α-Fe_2O_3	4	0.46		47
commercial Fe_3O_4 (300 nm)	4.8−8.0	1.08	1.56	28
commercial CuO nanoparticles	4		1.4	76
commercial TiO_2	4	4.11		47

As(V) and 37.5% As(III)) and Fe_3O_4-3 (28.6% As(V) and 19.2% As(III)). The better removal performances could be attributed to PDDA-induced high porous structure and increased surface area of the prepared Fe_3O_4 particles. All the above adsorption kinetic experimental data can be best fitted into a pseudo-second-order rate kinetic model, which is presented as follows

$$\frac{t}{q_t} = \frac{1}{k_2 q_e^{\,2}} + \frac{1}{q_e} t \tag{4}$$

where q_e and q_t are the amount of As(III) and As(V) adsorbed at equilibrium and at time t, respectively; k_2 is the rate constant of the pseudo-second-order model of adsorption (g mg^{-1} min^{-1}). The values of k_2 and q_e can be obtained by a plot of $(t)/(q_t)$ against t.

The conditions of As(V) and As(III) ions on the nanospheres were then characterized by XPS, as shown in Figure 8. Fe_3O_4 with arsenic adsorbed was collected by magnetic separation after the adsorption process (the initial arsenic concentration (As(V) and As(III): 5 mg L^{-1}). As shown in the full-range XPS spectra (Figure 8A), the appearance of As species and the increase of O intensity after arsenic adsorption both validate the arsenic adsorption on the Fe_3O_4 surface. XPS of Fe2p of all samples (Figure 8B) show the binding energies of $Fe2p^{1/2}$ at 724.4 eV and $Fe2p^{3/2}$ at 710.5 eV, which are closed to that of Fe_3O_4 reported.[47,73] XPS of As3d (Figure 8C) in Fe_3O_4 adsorbed As(V) shows a peak located at 45.1 eV, attributing to As(V)−O bonding, and that of As3d in Fe_3O_4

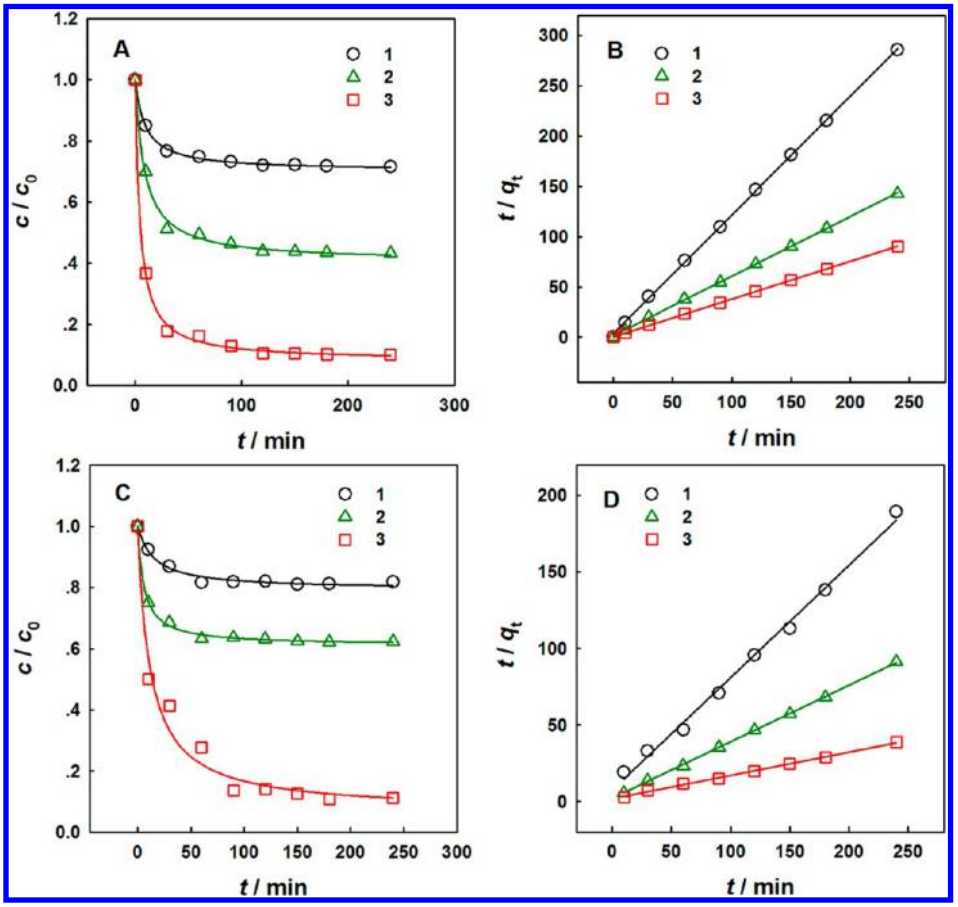

Figure 7. (A, C) Adsorption rate of As(V) and As(III) by Fe_3O_4-3 (1), Fe_3O_4-4 (2), and Fe_3O_4-5 (3), samples. (B, D) Pseudo-second-order kinetic plots for the adsorption of As(V) and As(III). (T = 25 °C; adsorbent doses = 0.5 g L^{-1}; pH = 5 ± 0.2).

dx.doi.org/10.1021/am403533v | ACS Appl. Mater. Interfaces XXXX, XXX, XXX−XXX

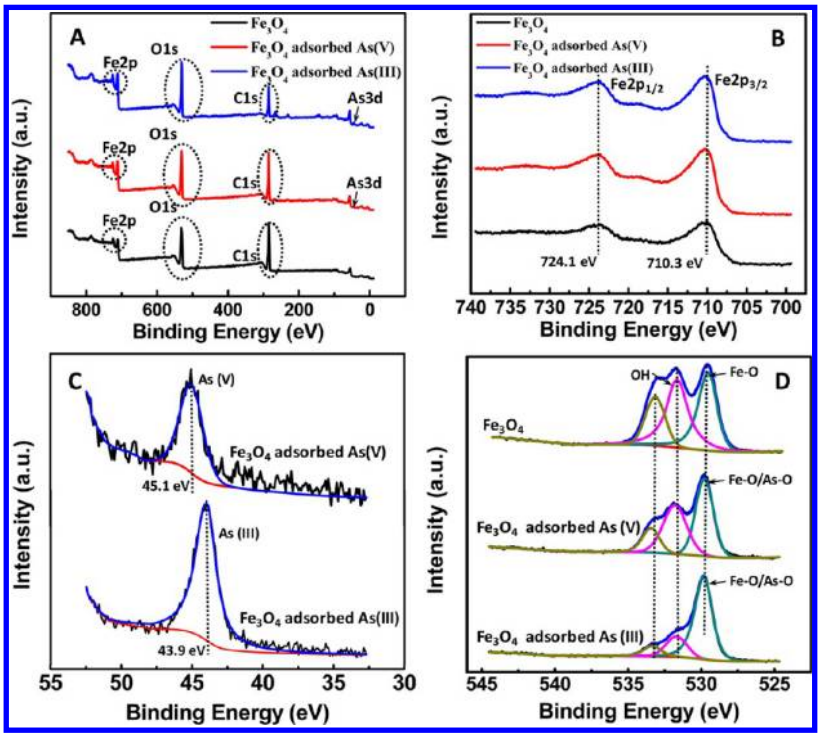

Figure 8. (A) Full-range, (B) Fe 2p, (C) As 3d, and (D) O 1s XPS spectra of several samples of interests including the Fe_3O_4, Fe_3O_4 adsorbed As(V), and Fe_3O_4 adsorbed As(III) particles.

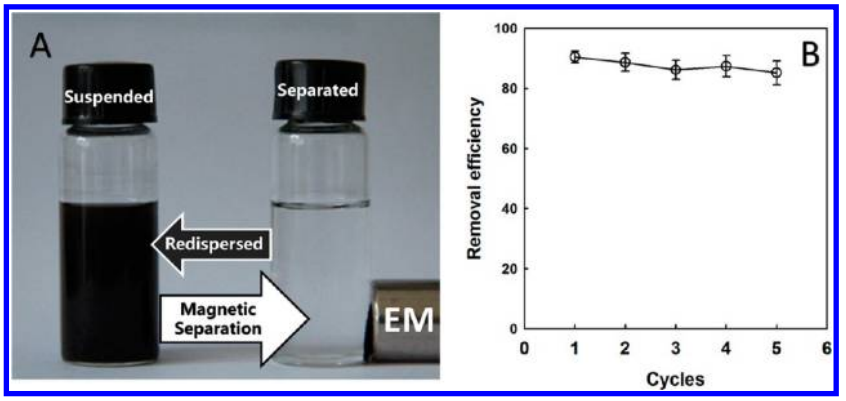

Figure 9. (A) Separation/redispersion property of Fe_3O_4-5 under external magnetic field (EM); (B) arsenic removal efficiency of Fe_3O_4-5 particles in different cycling numbers.

adsorbed As(III) shows fitted peak located at 43.9 eV, corresponding to As(III)-O, respectively.[14,78−81] The results confirmed no major differences in the valence state of the Fe and As species in arsenic adsorption. O1s XPS spectrum (Figure 8D) can be deconvoluted into peaks located at 530.0, 531.5, and 533.0 eV, which are attributed to oxygen in the lattice (e.g., Fe−O or As−O), oxygen atoms in the surface hydroxyl groups (H−O), and oxygen in the outermost layer of H_2O or CO_2 adsorbed.[14,79,82−84] The high peak intensity of H−O species of Fe_3O_4 confirms the existence of many hydroxyl groups on the surface of Fe_3O_4 spheres, which plays a vital important role in the arsenic removal.[14] Moreover, after arsenic adsorption, the shift of the O 1s binding energy to low energy, the proportion decrease of the H−O (531.5 eV) and the proportion increase of O in the lattice (530.0 eV) suggest that the adsorption mechanism was mainly ascribed to the substitution of Fe−OH groups by arsenic species.

Moreover, the quick magnetic separation, high desorption efficiency, and satisfactory recyclability of Fe_3O_4 have been investigated, as shown in Figure 9. Taking Fe_3O_4-5 as an example, the Fe_3O_4 suspension possesses merits of not only quick magnetic separation (within 5 s) but also unaffected redispersion property (the size of Fe_3O_4-5 measured via DLS before and after magnetic separation are in the range of 240−260 nm), which would greatly facilitate the application of Fe_3O_4 particles in low-cost and high efficient water remediation. After the recovery by magnetic separation, the Fe_3O_4 adsorbed arsenic compounds could be treated by untrasonification and then stirring in aqueous NaOH solution at pH 13 for 2 h, where upon they could be reused. It was found that the desorption efficiency was higher than 80% (86% for As(V) and 92% for As(III)), and the removal efficiency remained 85% after five cycles, which indicates the feasibility of regenerating the Fe_3O_4 adsorbent.

dx.doi.org/10.1021/am403533v | ACS Appl. Mater. Interfaces XXXX, XXX, XXX−XXX

4. CONCLUSION

A facile PDDA-modulated solvothermal method was proposed to synthesize porous hierarchical Fe_3O_4 particles with tunable grain size. As the PDDA dosage increases, grain size and particle size decrease, which yielded Fe_3O_4 hierarchical particles with enhanced surface area (from 7.05 to 32.75 $cm^3\ g^{-1}$) and promoted porosity (from 0.015 to 0.12 $cm^3\ g^{-1}$). Possible mechanism for PDDA-induced grain size tunable strategy can be ascribed to capping effect and high reaction medium viscosity which mediate the growth and assembly of grain. Due to the enhancement of surface area and high magnetism property, the prepared Fe_3O_4 display improved arsenic adsorption performance, superior efficiency in low-level arsenic removal, high desorption efficiency and satisfactory magnetic recyclability, which are very promising compared with commercial Fe_3O_4 particles. The porous Fe_3O_4 particles also process promising applications in other research field such as bioseparation, targeted drug delivery, and catalysis. Moreover, as generally believed that building blocks assemble into hierarchical materials, this methodology, modulating the property of building blocks, is facile and potentially general for controllably synthesizing hierarchical materials with high application performance.

■ ASSOCIATED CONTENT

Ⓢ Supporting Information

Additional information as noted in text. This material is available free of charge via the Internet at http://pubs.acs.org.

■ AUTHOR INFORMATION

Corresponding Author

*E-mail: Lychai@csu.edu.cn. Tel./Fax: +86 0731 88710171.

Author Contributions

The authors declare no competing financial interest. Ting Wang and Liyuan Zhang contributed equally to this work.

Notes

The authors declare no competing financial interest.

■ ACKNOWLEDGMENTS

We are thankful for the financial support by National Science Found for Distinguished Young Scholars of China (50925417), Chang Jiang Scholars Program (T2011116), National Public Welfare Research Project of Environmental Protection Industrial (2011467062), and Key Technology for the Remediation of Arsenic Pollution in Xiangjiang River Basin (K1201010-61).

■ REFERENCES

(1) Stone, R. *Science* **2008**, *321* (5886), 184−185.
(2) Yu, X.-Y.; Xu, R.-X.; Gao, C.; Luo, T.; Jia, Y.; Liu, J.-H.; Huang, X.-J. *ACS Appl. Mater. Interf.* **2012**, *4* (4), 1954−1962.
(3) Manning, B. A.; Hunt, M. L.; Amrhein, C.; Yarmoff, J. A. *Environ. Sci. Technol.* **2002**, *36* (24), 5455−5461.
(4) Gupta, A.; Yunus, M.; Sankararamakrishnan, N. *Ind. Eng. Chem. Res.* **2013**, *52* (5), 2066−2072.
(5) Gihring, T. M.; Druschel, G. K.; McCleskey, R. B.; Hamers, R. J.; Banfield, J. F. *Environ. Sci. Technol.* **2001**, *35* (19), 3857−3862.
(6) van Genuchten, C. M.; Addy, S. E.; Peña, J.; Gadgil, A. J. *Environ. Sci. Technol.* **2012**, *46* (2), 986−994.
(7) Hang, C.; Li, Q.; Gao, S.; Shang, J. K. *Ind. Eng. Chem. Res.* **2011**, *51* (1), 353−361.
(8) Lafferty, B. J.; Ginder-Vogel, M.; Sparks, D. L. *Environ. Sci. Technol.* **2011**, *45* (21), 9218−9223.
(9) Shipley, H. J.; Yean, S.; Kan, A. T.; Tomson, M. B. *Environ. Toxicol. Chem.* **2009**, *28* (3), 509−515.
(10) Kim, J.; Benjamin, M. M. *Water Res.* **2004**, *38* (8), 2053−2062.
(11) Coronell, O.; Mi, B.; Mariñas, B. J.; Cahill, D. G. *Environ. Sci. Technol.* **2012**, *47* (1), 420−428.
(12) Hristovski, K. D.; Westerhoff, P. K.; Crittenden, J. C.; Olson, L. W. *Environ. Sci. Technol.* **2008**, *42* (10), 3786−3790.
(13) Xu, W.; Wang, J.; Wang, L.; Sheng, G.; Liu, J.; Yu, H.; Huang, X.-J. *J. Hazard. Mater.* **2013**, *260* (0), 498−507.
(14) Cao, C.-Y.; Qu, J.; Yan, W.-S.; Zhu, J.-F.; Wu, Z.-Y.; Song, W.-G. *Langmuir* **2012**, *28* (9), 4573−4579.
(15) Yang, W.; Kan, A. T.; Chen, W.; Tomson, M. B. *Water Res.* **2010**, *44* (19), 5693−5701.
(16) Ai, Z.; Gao, Z.; Zhang, L.; He, W.; Yin, J. J. *Environ. Sci. Technol.* **2013**, *47* (10), 5344−5352.
(17) Wang, Y.; Zou, B.; Gao, T.; Wu, X.; Lou, S.; Zhou, S. *J. Mater. Chem.* **2012**, *22* (18), 9034−9040.
(18) Khin, M. M.; Nair, S.; babu Veluru, J.; Rajendiran, M.; Ramakrishna, S. *Energy Environ. Sci* **2012**, *5* (8), 8075−8109.
(19) Wang, Z.; Wu, L.; Zhou, J.; Cai, W.; Shen, B.; Jiang, Z. *J. Phys. Chem. C* **2013**, *117* (10), 5446−5452.
(20) Valtchev, V.; Tosheva, L. *Chem. Rev.* **2013**.
(21) Pang, X.; Zhao, L.; Han, W.; Xin, X.; Lin, Z. *Nat. Nanotechnol.* **2013**, *8* (6), 426−431.
(22) Liu, J.; Xu, J.; Che, R.; Chen, H.; Liu, M.; Liu, Z. *Chem.—Eur. J.* **2013**, *19* (21), 6746−6752.
(23) Wang, L.; Huang, Y.; Kan, A. T.; Tomson, M. B.; Chen, W. *Environ. Sci. Technol.* **2012**, *46* (10), 5422−5429.
(24) Yang, L.; Luo, S.; Li, Y.; Xiao, Y.; Kang, Q.; Cai, Q. *Environ. Sci. Technol.* **2010**, *44* (19), 7641−7646.
(25) Luo, X.-B.; Deng, F.; Min, L.; Luo, S.-L.; Guo, B.; Zeng, G.; Au, C. *Environ. Sci. Technol.* **2013**.
(26) Yavuz, C. T.; Mayo, J.; William, W. Y.; Prakash, A.; Falkner, J. C.; Yean, S.; Cong, L.; Shipley, H. J.; Kan, A.; Tomson, M. *Science* **2006**, *314* (5801), 964−967.
(27) Zeng, H.; Singh, A.; Basak, S.; Ulrich, K.-U.; Sahu, M.; Biswas, P.; Catalano, J. G.; Giammar, D. E. *Environ. Sci. Technol.* **2009**, *43* (5), 1373−1378.
(28) Yean, S.; Cong, L.; Yavuz, C.; Mayo, J.; Yu, W.; Kan, A.; Colvin, V.; Tomson, M. *J. Mater. Res.* **2005**, *20* (12), 3255−3264.
(29) Cotten, G. B.; Eldredge, H. B. *Sep. Sci. Technol.* **2002**, *37* (16), 3755−3779.
(30) Kelland, D. R. *IEEE Trans. Magn.* **1998**, *34* (4), 2123−2125.
(31) Mou, F.; Guan, J.; Ma, H.; Xu, L.; Shi, W. *ACS Appl. Mater. Interfaces* **2012**, *4* (8), 3987−3993.
(32) Ge, J.; Huynh, T.; Hu, Y.; Yin, Y. *Nano Lett.* **2008**, *8* (3), 931−934.
(33) Wei, Z.; Xing, R.; Zhang, X.; Liu, S.; Yu, H.; Li, P. *ACS Appl. Mater. Interfaces* **2012**, *5* (3), 598−604.
(34) Liu, G.; Deng, Q.; Wang, H.; Kang, S.; Yang, Y.; Ng, D. H.; Cai, W.; Wang, G. *Chem.—Eur. J.* **2012**, *18* (42), 13418−13426.
(35) Mou, F.; Guan, J.; Xiao, Z.; Sun, Z.; Shi, W.; Fan, X.-a. *J. Mater. Chem.* **2011**, *21* (14), 5414−5421.
(36) Wang, P.; Lo, I. *Water Res.* **2009**, *43* (15), 3727−3734.
(37) Xuan, S.; Wang, F.; Lai, J. M.; Sham, K. W.; Wang, Y.-X. J.; Lee, S.-F.; Yu, J. C.; Cheng, C. H.; Leung, K. C.-F. *ACS Appl. Mater. Interfaces* **2011**, *3* (2), 237−244.
(38) Ren, H.; Zhang, L.; Wang, T. T.; Li, L.; Wang, C. *Chem. Commun.* **2013**.
(39) Lou, X. W.; Archer, L. A. *Adv. Mater.* **2008**, *20* (10), 1853−1858.
(40) Liu, Y.; Wang, Y.; Zhou, S.; Lou, S.; Yuan, L.; Gao, T.; Wu, X.; Shi, X.; Wang, K. *ACS Appl. Mater. Interfaces* **2012**, *4* (9), 4913−4920.
(41) Wang, B.; Chen, J. S.; Wu, H. B.; Wang, Z.; Lou, X. W. *J. Am. Chem. Soc.* **2011**, *133* (43), 17146−17148.
(42) Peng, Q.; Dong, Y.; Li, Y. *Angew. Chem., Int. Ed.* **2003**, *42* (26), 3027−3030.
(43) Li, X.; Si, Z.; Lei, Y.; Li, X.; Tang, J.; Song, S.; Zhang, H. *CrystEngComm* **2011**, *13* (2), 642−648.

(44) Li, S.; Zhang, H.; Wu, J.; Ma, X.; Yang, D. *Cryst. Growth Des.* **2006**, *6* (2), 351−353.
(45) Liu, S.; Xing, R.; Lu, F.; Rana, R. K.; Zhu, J.-J. *J. Phys. Chem. C* **2009**, *113* (50), 21042−21047.
(46) Gao, Q.; Zhao, A.; Gan, Z.; Tao, W.; Li, D.; Zhang, M.; Guo, H.; Wang, D.; Sun, H.; Mao, R. *CrystEngComm* **2012**, *14* (14), 4834−4842.
(47) Zhong, L. S.; Hu, J. S.; Liang, H. P.; Cao, A. M.; Song, W. G.; Wan, L. J. *Adv. Mater.* **2006**, *18* (18), 2426−2431.
(48) Lian, J.; Duan, X.; Ma, J.; Peng, P.; Kim, T.; Zheng, W. *ACS Nano* **2009**, 3 (11), 3749−3761.
(49) Xuan, S.; Wang, Y.-X. J.; Yu, J. C.; Cham-Fai Leung, K. *Chem. Mater.* **2009**, *21* (21), 5079−5087.
(50) Zhu, Y.; Zhao, W.; Chen, H.; Shi, J. *J. Phys. Chem. C* **2007**, *111* (14), 5281−5285.
(51) Jia, B.; Gao, L. *J. Phys. Chem. C* **2008**, *112* (3), 666−671.
(52) Peng, S.; Sun, S. *Angew. Chem.* **2007**, *119* (22), 4233−4236.
(53) Yin, Y.; Rioux, R. M.; Erdonmez, C. K.; Hughes, S.; Somorjai, G. A.; Alivisatos, A. P. *Science* **2004**, *304* (5671), 711−714.
(54) Cheng, W.; Tang, K.; Qi, Y.; Sheng, J.; Liu, Z. *J. Mater. Chem.* **2010**, *20* (9), 1799−1805.
(55) Yang, H. G.; Zeng, H. C. *J. Phys. Chem. B* **2004**, *108* (11), 3492−3495.
(56) Hu, P.; Yu, L.; Zuo, A.; Guo, C.; Yuan, F. *J. Phys. Chem. C* **2008**, *113* (3), 900−906.
(57) Zhu, L.-P.; Xiao, H.-M.; Zhang, W.-D.; Yang, G.; Fu, S.-Y. *Cryst. Growth Des.* **2008**, *8* (3), 957−963.
(58) Chen, Y.; Xia, H.; Lu, L.; Xue, J. *J. Mater. Chem.* **2012**, *22* (11), 5006−5012.
(59) Yang, H. G.; Zeng, H. C. *Angew. Chem.* **2004**, *116* (44), 6056−6059.
(60) Wang, Y.; Zhu, Q.; Tao, L. *CrystEngComm* **2011**, *13* (14), 4652−4657.
(61) Zhang, S.; Shao, Y.; Liao, H.; Engelhard, M. H.; Yin, G.; Lin, Y. *ACS Nano* **2011**, *5* (3), 1785−1791.
(62) Ren, W.; Fang, Y.; Wang, E. *ACS Nano* **2011**, *5* (8), 6425−6433.
(63) Qin, C.; Chen, C.; Xie, Q.; Wang, L.; He, X.; Huang, Y.; Zhou, Y.; Xie, F.; Yang, D.; Yao, S. *Anal. Chim. Acta* **2012**, *720*, 49−56.
(64) Wang, S.; Yu, D.; Dai, L. *J. Am. Chem. Soc.* **2011**, *133* (14), 5182−5185.
(65) Wang, S.; Yu, D.; Dai, L.; Chang, D. W.; Baek, J.-B. *ACS Nano* **2011**, *5* (8), 6202−6209.
(66) Mohan, D.; Pittman, C. U., Jr. *J. Hazard. Mater.* **2007**, *142* (1), 1−53.
(67) Addo Ntim, S.; Mitra, S. *J. Chem. Eng. Data* **2011**, *56* (5), 2077−2083.
(68) Katsoyiannis, I. A.; Zouboulis, A. I. *Water Res.* **2002**, *36* (20), 5141−5155.
(69) Fan, T.; Pan, D.; Zhang, H. *Ind. Eng. Chem. Res.* **2011**, *50* (15), 9009−9018.
(70) Liu, Z.-h.; Yang, X.; Makita, Y.; Ooi, K. *Chem. Mater.* **2002**, *14* (11), 4800−4806.
(71) Liu, K.; Zhang, J.; Yang, G.; Wang, C.; Zhu, J.-J. *Electrochem. Commun.* **2010**, *12* (3), 402−405.
(72) Zhu, M.; Diao, G. *J. Phys. Chem. C* **2011**, *115* (39), 18923−18934.
(73) Zhu, H.; Hou, C.; Li, Y.; Zhao, G.; Liu, X.; Hou, K.; Li, Y. *Chem. Asian J.* **2013**, *8* (7), 1447−1454.
(74) Lesniak, W.; Bielinska, A. U.; Sun, K.; Janczak, K. W.; Shi, X.; Baker, J. R.; Balogh, L. P. *Nano Lett.* **2005**, *5* (11), 2123−2130.
(75) Cumberland, S. A.; Lead, J. R. *J. Chromatogr. A* **2009**, *1216* (52), 9099−9105.
(76) Cao, A.-m.; Monnell, J. D.; Matranga, C.; Wu, J.-m.; Cao, L.-l.; Gao, D. *J. Phys. Chem. C* **2007**, *111* (50), 18624−18628.
(77) Yu, X.-Y.; Luo, T.; Jia, Y.; Zhang, Y.-X.; Liu, J.-H.; Huang, X.-J. *J. Phys. Chem. C* **2011**, *115* (45), 22242−22250.
(78) Kanel, S. R.; Greneche, J.-M.; Choi, H. *Environ. Sci. Technol.* **2006**, *40* (6), 2045−2050.
(79) Nesbitt, H.; Muir, I. *Mineral. Petrol.* **1998**, *62* (1−2), 123−144.
(80) Gomes, J. A.; Daida, P.; Kesmez, M.; Weir, M.; Moreno, H.; Parga, J. R.; Irwin, G.; McWhinney, H.; Grady, T.; Peterson, E. *J. Hazard. Mater.* **2007**, *139* (2), 220−231.
(81) Chen, B.; Zhu, Z.-L.; Ma, J.; Qiu, Y.-L.; Chen, J. *J. Mater. Chem. A* **2013**, *1* (37), 11355−11367.
(82) Wielant, J.; Hauffman, T.; Blajiev, O.; Hausbrand, R.; Terryn, H. *J. Phys. Chem. C* **2007**, *111* (35), 13177−13184.
(83) Ramos, M. A.; Yan, W.; Li, X.-q.; Koel, B. E.; Zhang, W.-x. *J. Phys. Chem. C* **2009**, *113* (33), 14591−14594.
(84) Lim, S.-F.; Zheng, Y.-M.; Chen, J. P. *Langmuir* **2009**, *25* (9), 4973−4978.
(85) Zheng, J. Y.; Wang, X.; Li, W.; Cao, Z.; Wang, H.; Zhang, C.; Song, W.-G.; Ma, Y.; Yao, J. *CrystEngComm* **2012**, *14* (22), 7616−7620.